IOP Publishing J. Phys. Photonics 2 (2020) 04LT01 https://doi.org/10.1088/2515-7647/abb3b5

Journal of Physics: Photonics

OPEN ACCESS

RECEIVED
4 June 2020

REVISED
27 July 2020

ACCEPTED FOR PUBLICATION
28 August 2020

PUBLISHED
1 October 2020

LETTER

19-element vertical cavity surface emitting laser arrays with inter-vertical cavity surface emitting laser ridge connectors

Nasibeh Haghighi[1], **Philip Moser**[1], **Martin Zorn**[2] **and James A Lott**[1]

[1] Institute of Solid-State Physics, Technical University Berlin, Berlin, Germany
[2] JENOPTIK Optical Systems GmbH, Berlin, Germany

E-mail: nasibeh.haghighi@tu-berlin.de

Keywords: vertical cavity surface emitting laser, optical interconnect, optical communication

Abstract

We achieve record concurrent combinations of bandwidth (18 GHz), optical output power (150 mW), and wall plug efficiency (30%) with a unique arrangement of 19-element, electrically parallel 980 nm vertical cavity surface emitting laser (VCSEL) arrays. We use a new two-dimensional, quasi honeycomb geometry with inter-VCSEL ridge connectors—made nonconducting by selective thermal oxidation—to improve heat dissipation and facilitate a single top surface anode contact. Via on-wafer probing we perform static and dynamic measurements over the wide temperature range of 23 °C to 85 °C and extract, report, and discuss key array figures-of-merit.

1. Introduction

Fifth generation (5G) information, sensory, and communication systems promise a plethora of real-time life enhancing tools for: immersive experiences, mobility, safety, health, commerce, education, transportation, and leisure. The vertical cavity surface emitting laser (VCSEL) is a key enabler for several 5G optical wireless communication applications including: line of sight backhaul, last-mile and local area (fixed, temporary, mutable) mesh networks, secure personal area networks, and Internet of Things sensing and connectivity. The 5G standard specifies data rates of 5 to 20 gigabit-per-second (Gb s^{-1}) but allows untethered bit rate and bandwidth increases and fluctuations (as new technology is invented, produced, and deployed) to fill a massive variety of flexible, ubiquitous, and esoteric applications including: free space optical (FSO) inter-rack interconnects in data centres [1]; FSO line-of-sight communication links [2]; light-fidelity systems [3]; (outer) space optical communication [4]; time-of-flight (ToF) sensing [5, 6]; three-dimensional (3D) imaging [6]; and light detection and ranging (LiDAR) [7].

We investigate the device physics of two-dimensional (2D) VCSEL arrays for possible (future) use in FSO communication or sensing systems. Comparing VCSEL arrays is quite difficult as device geometry (top versus bottom emission, optically coupled versus optically uncoupled elements, variable number and arrangement of elements, etc.), emission wavelength, and performance targets vary significantly. While reports of VCSEL-based FSO communication links focus on link distance, data transmission rate, and bit error ratio (BER) (e.g. 10 Gb s^{-1} at a BER of 1×10^{-9} across 3 m [1]), reports of VCSEL arrays for ToF sensing, 3D imaging, and/or LiDAR focus on pulsed optical output power (and duty cycle), rise and fall time (e.g. tens of ps [6]), far field beam pattern (e.g. a donut or top hat intensity profile, large or small divergence angle), and a novel device processing and/or packaging scheme [5–7]. We focus on trade-offs between optical output power, bandwidth (leading to potentially high bit rates), and efficiency.

We seek arrays with optical output power exceeding 100 mW (for short to medium free space distances) and simultaneously the highest possible modulation bandwidth (enabling error-free data transmission at 20 Gb s^{-1} or higher) and the highest possible wall plug efficiency (WPE). We use 980 nm since eye safe, cylindrical or conical optical data and sensing beams at wavelengths of ~940–1090 nm (up to ~1300–1600 nm) are envisioned for free space 5G systems, and 980 nm is simply a convenient emission wavelength for basic VCSEL research and development. We scale up the optical output power via a novel

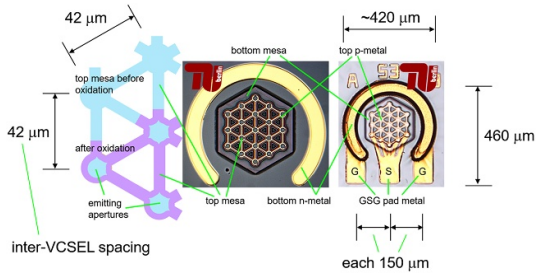

Figure 1. Partial schematic (left) and optical microscope images of a 19-element, electrically parallel 980 nm VCSEL array: (middle) after the n-metal deposition step; and (right) fully processed.

interconnected (electrically parallel) VCSEL array design with inter-VCSEL ridge connectors to help dissipate heat and to help lower series resistance [8,9]. Here we present our first study of our new 19-element 980 nm arrays—focusing on extracting common laser diode figures-of-merit from room temperature (RT ~ 23 °C) to 85 °C.

Our state-of-the-art, 19-element, VCSEL arrays exhibit a bandwidth (f_{3dB}) of 18 GHz, a continuous wave (CW) optical output power (L) of 150 mW, a WPE of 30%, and (test) data transmission at 20 and 25 Gb s^{-1}. For comparison, the pioneering work in 2005 by Fuji Xerox (Japan) on 2x2, 3x3, and 4x4 VCSEL arrays emitting at 850 nm yielded cone-shaped FSO beams capable of sending digital data at 2.5 Gb s^{-1} [10]. Subsequent work in 2010 on VCSEL arrays—wherein the authors sought the simultaneous combination of high L and high f_{3dB} (and ideally high WPE) yielded a 28-element, 980 nm array with f_{3dB} ~ 7.6 GHz, a peak CW L ~ 150 mW, and a WPE ~ 12% [11]. Fresh work in 2020 on a 9-element, 940 nm array yielded a 10 GHz bandwidth, 62.4 mW of peak CW optical output power, and a WPE of ~20% [12]. The authors in [11, 12] did not report data transmission results.

2. Geometry and fabrication

We fabricate electrically parallel, optically uncoupled VCSEL arrays using the epitaxial VCSEL wafers described in [8, 9]. In figure 1 we unveil optical microscope images of our 19-VCSEL array. We deposit 3.5 μm wide top p-metal (Ti/Au) on the wafer surface in a 2D quasi honeycomb pattern (a 2D hexagonal close pack lattice), where a single VCSEL is surrounded by a 6-VCSEL regular hexagonal ring, in turn surrounded by a 12-VCSEL regular hexagonal ring. The top mesa consists of 22 μm diameter circular pillars interconnected with 9.5 μm wide rectangular (inter-VCSEL) ridge connectors between nearest neighbours. Our ridge connectors improve heat dissipation but slightly increase oxide capacitance and reduce the small signal modulation bandwidth. We demonstrate this phenomenon (not reported here) by processing and characterizing VCSEL arrays: with and without ridge connectors; with different inter-VCSEL pitch; and with a different number of elements. We will include an extensive comparative study of different VCSEL array geometries in a future publication. The 3.5 μm wide circular horseshoe anode contact rings and interconnecting metal lines along the ridges reside 3 μm from top mesa edges. The inter-VCSEL pitch is 42 μm.

We etch a single top mesa (into a web of interconnected circular pillars) from the surface through the p-doped distributed Bragg reflector (DBR) mirror and past two oxide aperture layers that surround the 0.5λ (optically thick) VCSEL optical cavity. Via wet (using water vapour) selective thermal oxidation at 420 °C and 50 mbar we fully oxidize the two Al-rich layers under the ridges (for ~111 min at a lateral oxidation rate ~0.0658 μm min^{-1} [8])—to prevent current flow across the VCSEL active pn junction along the ridges. Simultaneously we form near-circular oxide apertures in the circular pillars that may include tiny cusps pointed outward along each ridge connector as illustrated in figure 1. The variation in ϕ within an array is, we believe, negligible. Via spectral emission measurements on previous triple and septuple VCSEL arrays [8] we found no discernible difference between the emission spectra of the individual VCSELs (measured one by one).

We next etch a second mesa (in the shape of a regular hexagon with side lengths of 115 μm) down through the bottom (n)DBR into the (n+)GaAs ohmic contact layer and deposit ohmic n-metal (Ni/AuGe/Ni/Au) in a 46.3 μm wide circular horseshoe (see figure 1). We complete the processing by planarising the wafer using photosensitive bisbenzocyclobutene (BCB), developing (removing) BCB vias in the shape of a circular horseshoe over the n-metal (and in the shape of a circle over each VCSEL emitting aperture), and depositing co-planar ground-signal-ground (GSG) metal (Cr/Au) contact pads for on wafer

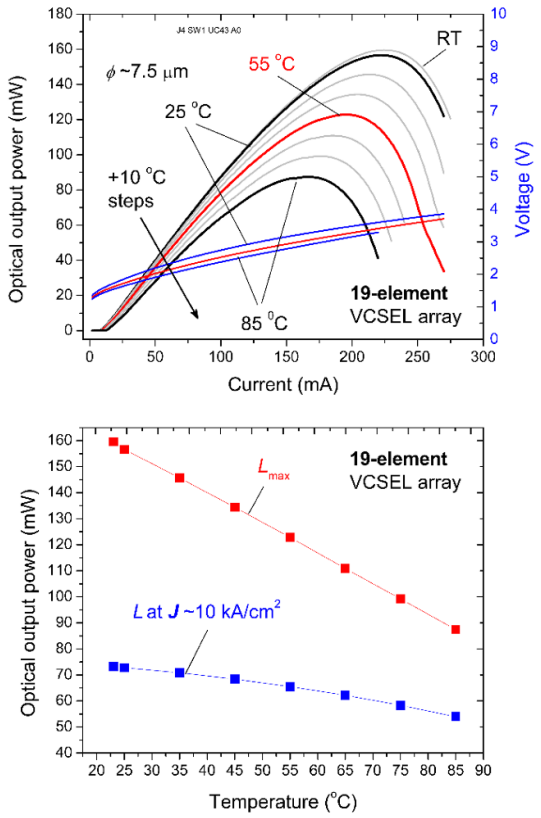

Figure 2. Static characteristics of a 19-element 980 nm VCSEL array with $\phi \sim 7.5$ μm at 23 °C to 85 °C including the: (top) CW optical output power (L) and voltage (V) versus bias current (I); and (bottom) maximum optical output power (I_{max}) and L at $\boldsymbol{J} \sim 10$ kA cm^{-2}.

static and dynamic device testing with high frequency co-planar GSG probes with 150 μm pin-to-pin spacing.

3. Static testing

To determine the temperature (T) stability of our 19-element array we measure the CW *LIV* characteristics from ~23 °C–85 °C via a platen heater. In figure 2 (top) we plot CW *LIV* data versus T. At 25 °C the maximum CW optical output power (L_{max}) is 157 mW (at $I \sim 225$ mA) and at 85 °C L_{max} is 87 mW (at $I \sim 175$ mA)—a power decrease of 45%. In figure 2 (bottom) we plot L_{max} and L at a bias current density $\boldsymbol{J} \sim 10$ kA cm^{-2} (a reference rule-of-thumb (maximum) bias for reliable oxide aperture VCSELs; see [13]) both versus T. We neglect unoxidized cusp areas and compute $\boldsymbol{J} = I/[19{\cdot}\pi(\phi/2)^2]$, where ϕ is the oxide aperture diameter.

In figure 3 we show the *LI* data (from figure 2) close to threshold, and we plot the threshold current (I_{th}) and the threshold current density ($\boldsymbol{J}_{th}$) versus T. We observe I_{th} and $\boldsymbol{J}_{th}$ minima at ~35 °C—the approximate temperature where the VCSEL etalon (fundamental LP01 mode resonance) aligns with the peak of the QW gain. The I_{th} is ~8 mA at 25 °C and increases by 63% to ~13 mA at 85 °C.

We next extract the CW WPE (expressed as a percent; WPE $= 100{\cdot}L/[V{\cdot}I]$) from our static *LIV* data and graph the maximum WPE in figure 4. The maximum WPE varies from 36.6% at 25 °C to 30% at 85 °C. Our WPE matches state-of-the-art values of high bandwidth VCSELs [14, 15] and of a single $\phi \sim 7.5$ μm reference VCSELs adjacent to the arrays [8].

We extract two additional parameters of interest from the static *LIV* data: (1) the *LI* slope maxima ($\eta_{LI} = \Delta L/\Delta I$, in W/A); and (2) the unitless external differential quantum efficiency ($\eta_{ex} = (q\lambda/hc){\cdot}(\Delta L/\Delta I)$, where h is Planck's constant, λ is the emission wavelength, and c is the speed of light). We include plots of these parameters versus T in figure 4, and for reference we include the CW magnitudes of L, η_{LI}, and η_{ex} at $\boldsymbol{J} \sim 10$ kA cm^{-2}.

In figure 5 (top) we illustrate—via a 2D waterfall plot—the RT CW spectral emission for the 19-element array at: $I = 5$ mA (below threshold), $I = 85$ mA ($\boldsymbol{J} \sim 10.1$ kA cm^{-2}), and $I = 125$ mA ($\boldsymbol{J} \sim 14.9$ kA cm^{-2}).

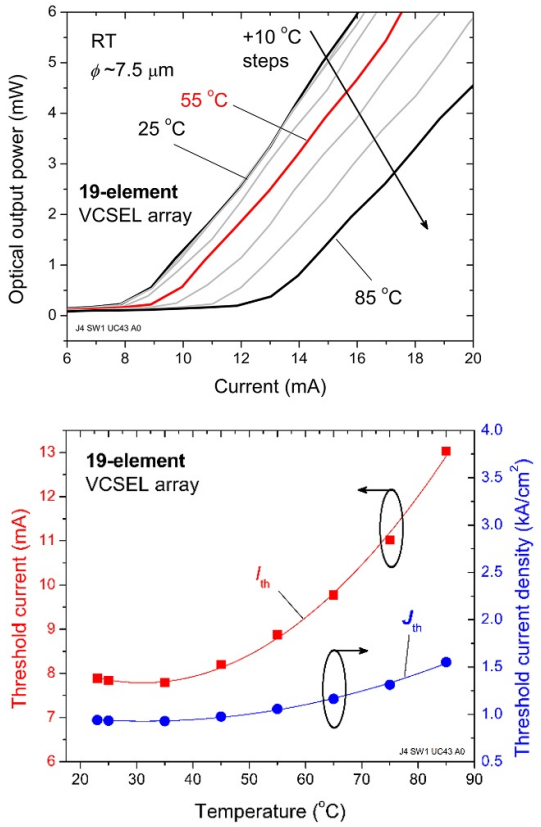

Figure 3. For the VCSEL array with $\phi \sim 7.5$ μm in figure 2: (top) the *LI* characteristics near threshold versus T; and (bottom) the threshold current (I_{th}) and threshold current density ($\boldsymbol{J}_{th}$) versus T.

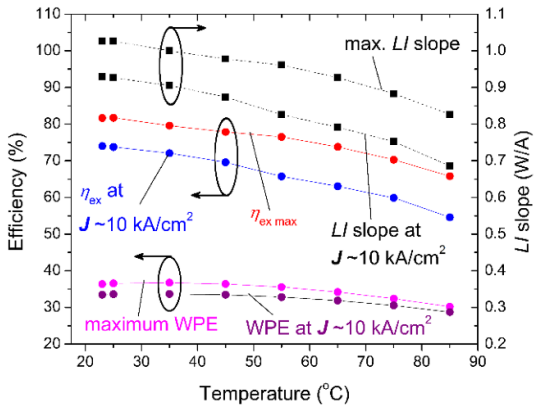

Figure 4. Figures of merit for a 19-element 980 nm VCSEL array with $\phi \sim 7.5$ μm at $T = 23$ °C to 85 °C including the: maximum *LI* slope efficiency; the maximum external differential quantum efficiency ($\eta_{ex\,max}$); the maximum WPE; and the same three parameters at $\boldsymbol{J} \sim 10$ kA cm^{-2}.

We record the red shift of the fundamental (LP01) optical mode from $I = 5$ mA ($\lambda_{LP01} = 985.7$ nm) to $I = 215$ mA ($\lambda_{LP01} = 994.7$ nm) in 10 mA steps. We compute $\Delta\lambda/\Delta P_{diss}$ (0.0137 nm mW^{-1}), where the dissipated power $P_{diss} = I{\cdot}V{-}L$. In figure 5 (bottom) we graph the emission spectra of our x19 array at 25 °C to 85 °C in 10 °C steps and track the subsequent linear shift in the fundamental LP01 mode wavelength. We find $\Delta\lambda/\Delta T = 0.0697$ nm °C^{-1}. To minimize current-induced self-heating (joule heating) we measure each CW emission spectra close to the threshold current.

The thermal resistance of our 19-element array is thus $R_{th,x19} = (\Delta\lambda/\Delta P_{diss})/(\Delta\lambda/\Delta T) = 0.2$ °C mW^{-1} ($R_{th} \sim 3.8$ °C mW^{-1} per VCSEL). For comparison, $R_{th} = 1.5$ °C mW^{-1} for a Cu plated $\phi \sim 7$ μm single top emitting 980 nm VCSEL [16], and $R_{th} = 0.03$ °C mW^{-1} for a $\phi \sim 18$ μm 28-element flip-bonded substrate emitting 980 nm VCSEL array [11]. A typical R_{th} value for a single VCSEL with $\phi \sim 50$ μm is ~0.1 °C mW^{-1}, which exponentially increases to above 1 °C mW^{-1} as ϕ decreases below 10 μm [17].

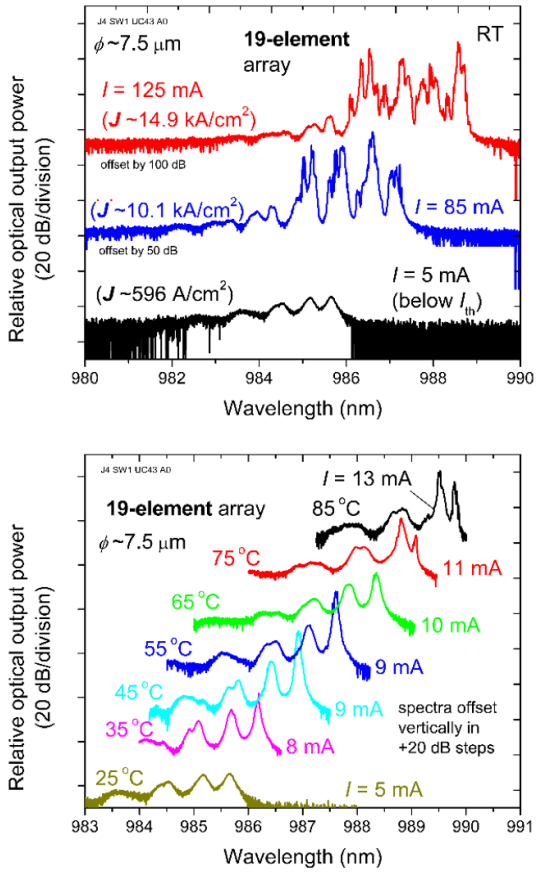

Figure 5. Optical emission spectra (electroluminescence) of a 19-element (x19) 980 nm VCSEL array with $\phi \sim 7.5$ μm as 2D waterfall plots: (top) at room temperature (RT) for $I = 5$, 85, and 125 mA; and (bottom) within 0.5 mA of I_{th} from 25 to 85 °C in 10 °C steps.

4. Dynamic testing

To determine the dynamic properties of our 19-element VCSEL array we measure the small signal frequency response (the real and imaginary parts of the 2-port scattering parameter S21 versus frequency) at different bias currents (I) from near threshold to the LI rollover and in a wide temperature range from 25 °C to 85 °C. Both the threshold current and the rollover current vary with ambient T (which we set by heating the probe station platen). For example, we measure S21 versus frequency at bias currents from $I = 10$ mA to: 225 mA at 25 °C; 200 mA at 55 °C; and 170 mA at 85 °C, all using 10 mA current steps. We employ our standard S21 measurement method using an HP 8722 C Vector Network Analyzer, a cleaved-end OM1 multiple-mode optical fibre (MMF), and a New Focus Model 1434 photodetector with a bandwidth of 25 GHz, and the curve fitting equation in [9]. We obtain parameters of interest including the D-Factor, the modulation current efficiency factor (MCEF), and the −3 dB bandwidth (f_{3dB}) versus I and $\boldsymbol{J}$.

In figure 6 we graph |S21| at 25 °C, 55 °C, and 85 °C for $\boldsymbol{J} \sim 10$ kA cm^{-2}. We set |S21| to the reference level 0 dB at 0 Hz. The slight dip in the |S21| between 0 and 7 GHz is likely due to thermal lensing and spatial nonuniformity of the transverse modes as described in [18]. The frequency response curve peaking is ~3 dB above the level at 0 GHz at 25 °C and decreases to only ~1 dB at 85 °C, due to the expected increase in the damping factor with increasing T.

In figure 7 (top) we plot f_{3dB} versus $\boldsymbol{J}$ at 25 °C, 55 °C, and 85 °C. In figure 7 (bottom) we plot the maximum f_{3dB} ($f_{3dB\,max}$) and the f_{3dB} at $\boldsymbol{J} \sim 10$ kA cm^{-2} versus T from 25 °C to 85 °C in 10 °C steps. The maximum f_{3dB} (18.3 GHz at 25 °C; 17.6 GHz at 55 °C; and 15.6 GHz at 85 °C) lie just above $\boldsymbol{J} \sim 15$ kA cm^{-2}, with only an ~2 GHz decrease in each at $\boldsymbol{J} \sim 10$ kA cm^{-2}. We reach the maximum f_{3dB} (which remains nearly constant) as $\boldsymbol{J}$ varies from ~16–20 kA cm^{-2}. Our bandwidths are reasonably temperature invariant—as desired. The maximum f_{3dB} at 85 °C is only ~3 GHz lower than at 25 °C (when $\boldsymbol{J} \sim 16$ to 20 kA cm^{-2}). We calculate the D-Factor ($f_R = D \cdot (I-I_{th})^{1/2}$) and the MCEF ($f_{3dB} = \text{MCEF} \cdot (I-I_{th})^{1/2}$)

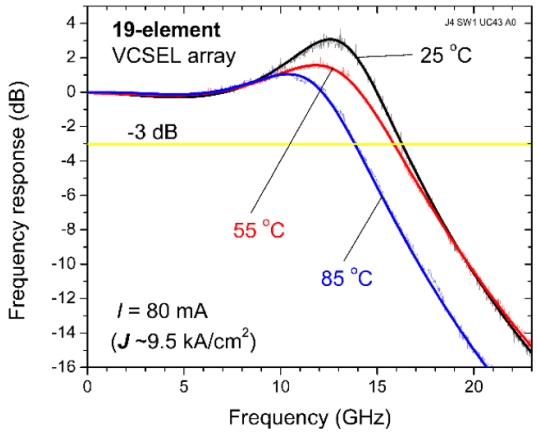

Figure 6. Small signal modulation frequency response curves and associated curve fits at $\boldsymbol{J} \sim 10$ kA cm^{-2} for the 19-element 980 nm VCSEL array with $\phi \sim 7.5$ μm at: 25 °C (black curves), 55 °C (red curves), and 85 °C (blue curves).

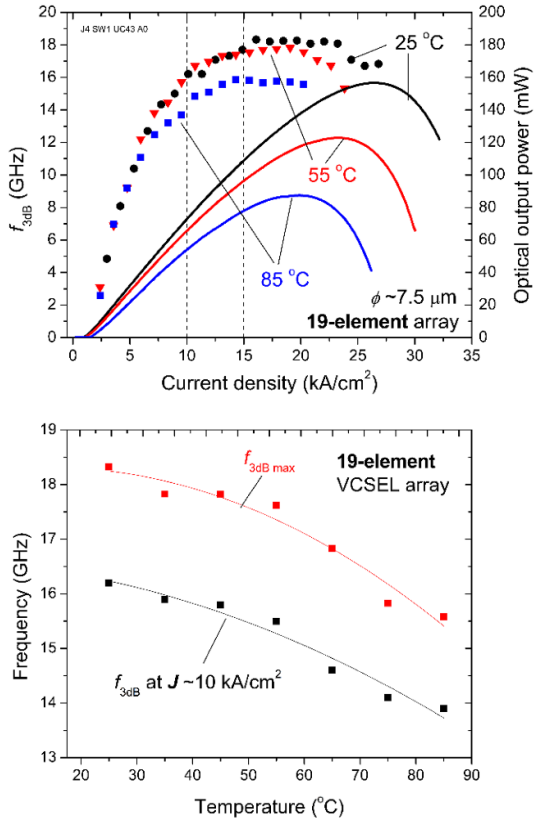

Figure 7. For a 19-element 980 nm VCSEL array with $\phi \sim 7.5$ μm: (top) small signal modulation −3 dB bandwidth (f_{3dB}) and optical output power (L curves) both versus current density ($\boldsymbol{J}$) at 25 °C (black circles and black curve), 55 °C (red triangles and red curve), and 85 °C (blue squares and blue curve); and (bottom) maximum bandwidth ($f_{3dB\,max}$) and f_{3dB} at $\boldsymbol{J} \sim 10$ kA cm^{-2} versus T at 25 °C to 85 °C.

versus T by first determining I_{th} from a linear plot of $f_R{}^2$ versus I at small I. We find that D and MCEF decrease from 1.7 to 1.5 and 1.8 to 1.6 GHz (mA)$^{-1/2}$, respectively, as T varies from 25 °C to 85 °C.

To demonstrate the potential of our arrays as possible sources for optical interconnects we perform large signal modulation data transmission experiments at RT. We place the cleaved end of an OM1 multiple mode optical fibre patch cord a few millimetres above the VCSEL array to capture a mix of the optical emission from all 19 VCSELs. We achieve the same bit error ratio (BER) test results when we vary the position of the collecting optical fibre around the immediate vicinity of the emitting array. To collect all the emitted light—we would need a set of lenses to focus the optical emission into the MMF or to shape the emission into a beam for travel across free space into a photoreceiver. These FSO communication experiments are beyond our scope but well suited for future work with a communication systems research group.

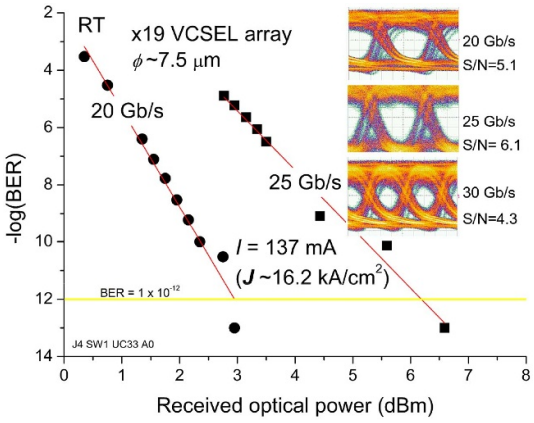

Figure 8. Bit error ratio (BER) versus received optical power for a 19-element 980 nm VCSEL array with $\phi \sim 7.5\ \mu$m. We use a cleaved-end OM1 MMF and a CW bias current of 137 mA ($\boldsymbol{J} \sim 16.2$ kA cm^{-2}). Insets: optical eye diagrams and their signal to noise (S/N) ratios.

We first set the attenuation to 0 dB and optimize the optical eye diagram at 25 Gb s^{-1}—we find the largest possible eye opening and signal to noise (S/N) ratio—by tweaking the CW bias current. We transmit digital data for at least 30 s and record the BER. We use 2-level, nonreturn to zero, pulse amplitude modulation with a pseudorandom binary (PRB) sequence of word length of 2^7–1. Thus at 25 Gb s^{-1} we transmit ≥750 billion bits (≥5.9 billion PRB sequences) then record the BER.

In figure 8 we plot the BER versus the received optical power at $I = 137$ mA ($\boldsymbol{J} \sim 16.2$ kA cm^{-2}) for data transmission at 20 and 25 Gb s^{-1}. We record 0 errors when we set the optical attenuation to 0 dB—we therefore set the BER to 1×10^{-13}. We measure corresponding S/N ratios at 20 and 25 Gb s^{-1} equal to 5.1 and 6.1 (see the eye diagrams in figure 8). When we connect a variable optical attenuator (JDSU OLA-54) between the OM1 fibre and the photoreceiver (adding insertion loss) the BER increases to $>1 \times 10^{-11}$. We obtain open eye diagrams at 30 Gb s^{-1} with 0 optical attenuation but the BER exceeds 1×10^{-12}.

5. Conclusion

Our top-surface-emitting novemdecuple (19-element) VCSEL arrays are potential light sources for applications requiring low to moderate optical power (easily up to ~120 mW) and concurrently reasonably high bandwidth (~16–18 GHz). Our unique array design includes inter-VCSEL ridge connectors (effectively yielding one top mesa structure but with independent nonconducting (in the vertical direction) ridges and conducting VCSEL apertures) which serve to distribute heat and thus we believe help to stabilize the array performance. The ridges likely allow us to place the VCSELs closer together before thermal crosstalk degrades the array performance.

We may scale-up (or scale-down) the optical output power by increasing (decreasing) the oxide aperture diameters or by adding (removing) VCSEL elements. Adding elements will generally decrease the bandwidth and vice versa for our current top-surface-emitting array design. The key is to optimize the array design for the given application, emphasizing the power, bandwidth, efficiency, or a trade-off of the three to meet the performance requirement.

Acknowledgments

The German Research Foundation funds this work via the Collaborative Research Centre 787.

ORCID iD

James A Lott https://orcid.org/0000-0003-4094-499X

References

[1] Ali W, Cossu G, Gilli L, Ertunc E, Messa A, Sturniolo A and Ciaramella E 2019 *IEEE Photonics Technol. Lett.* **31** 805
[2] Liverman S, Bialek H, Natarajan A and Wang A 2020 *J. Lightwave Technol.* **38** 1659
[3] Yeh C-H, Yang Y-C, Chow C W, Chen Y-W and Hsu T-A 2020 *J. Lightwave Technol.* **38** 5728–32
[4] Goorjian P M 2020 *Proc. SPIE 11272, Free-Space Laser Communications XXXII, Photonics West (San Francisco, CA)* p 1127214

[5] Moench H, Gronenborn S, Gu X, Gudde R, Herper M, Kolb J, Miller M, Smeets M and Weigl A 2019 *Proc. SPIE 10938 Vertical-Cavity Surface-Emitting Lasers XXIII, Photonics West (San Francisco, CA)* p 109380E
[6] Khan Z, Shih J-C, Chao R-L, Tsai T-L, Wang H-C, Fan G-W, Lin Y-C and Shi J-W 2020 *Optica* **7** 267
[7] Warren M E, Podva D, Dacha P, Block M K, Helms C J, Maynard J and Carson R F 2018 *Proc. SPIE 10552 Vertical-Cavity Surface-Emitting Lasers XXII, Photonics West* San Francisco, CA p 105520E
[8] Haghighi N, Moser P and Lott J A 2019 *IEEE J. Sel. Top. Quantum Electron.* **25** 495
[9] Haghighi N, Moser P and Lott J A 2020 *J. Lightwave Technol.* **38** 3387
[10] Yoshikawa M, Murakami A, Sakurai J, Nakayama H and Nakamura T 2005 High power VCSEL devices for free space optical communications *Proc. Electronic Components and Technology (ECTC)* (Piscataway, NJ: IEEE) pp 1353–58
[11] Safaisini R, Joseph J R and Lear K L 2010 *IEEE J. Quantum. Electron.* **46** 1590
[12] Khan Z, Shih J-C, Chang Y-H and Shi J-W 2020 *Proc. Conference on Lasers and Electro-Optics (CLEO) (San Jose, CA)* p ATh1K
[13] Hawkins B M, Hawthorne R A, Guenter J K, Tatum J A and Biard J R 2002 *Proc. 52nd Electronics Components and Technology Conf.* (*San Diego, CA*) p 540
[14] Haglund E, Westbergh E P, Gustavsson J S, Haglund E P and Larsson A 2016 *J. Lightwave Technol.* **34** 269
[15] Moser P 2016 *Energy-Efficient VCSELs for Optical Interconnects* (Berlin: Springer)
[16] Al-Omari A N, Carey G P, Hallstein S, Watson J P, Dang G and Lear K L 2006 *IEEE Photonics Technol. Lett.* **18** 1225
[17] Grabherr M, Miller M, Jäger R, Michalzik R, Martin U, Unold H J and Ebeling K J 1999 *IEEE J. Sel. Top. Quantum Electron.* **5** 495
[18] Liu Y, Ng W C, Klein B and Hess K 2003 *IEEE J. Quantum. Electron.* **39** 99